Experimental Observation of Single Skyrmion Signatures in a Magnetic Tunnel Junction

N. E. Penthorn,[1] X. Hao,[2] Z. Wang,[2] Y. Huai,[2] and H. W. Jiang[1,*]

[1]*Department of Physics and Astronomy, University of California, Los Angeles, California 90095, USA*
[2]*Avalanche Technology, Fremont, California 95438, USA*

We have deterministically created a stable topological spin texture in magnetic tunnel junctions (MTJ) by using pulsed or microwave currents. The spin texture is characterized by a field-dependent intermediate resistance state and a new magnetic resonance. Micromagnetic simulations show that the observations are consistent with the nucleation of a single skyrmion, facilitated by a spatially nonuniform stray field. The unique resonance spectrum is identified as the skyrmion breathing mode and a skyrmion diameter of 75 nm is estimated. This work shows the possibility to create skyrmions in MTJs without the Dzyaloshinskii-Moriya interaction and could lead to noninvasive, on-chip skyrmion measurement.

Research on magnetic skyrmions, localized topological spin textures in magnetic materials, has gained momentum in recent years due to the technological advancement of magnetic films and the possible application of skyrmions in information storage and processing. For memory applications, much experimental attention has been given to the racetrack architecture where skyrmions are shuttled along a thin magnetic film with an applied current [1]. Moreover, there have been computational studies demonstrating the use of skyrmions for logic gates [2], artificial synapses for neuromorphic computing [3], and harboring Majorana bound states for topological quantum computing [4]. Because of low creation energy, robustness to defects and compact size, magnetic skyrmions have considerable potential in the field of spintronics.

The majority of experimental research has been restricted to multi-skyrmion states in thin magnetic films, but there is substantial interest in device settings where individual skyrmions need to be generated and read out on chip. A popular design solution for electrical creation and detection of skyrmions is the magnetic tunnel junction (MTJ) [5,6], as MTJs are arguably the most promising spintronics devices developed in recent years for data storage, sensing, and logic computation. Tunnel magnetoresistance (TMR) is an excellent way to sensitively measure the magnetization of an MTJ's constituent magnetic layers, and the writing energy required to create or annihilate a magnetic skyrmion in the free layer of an MTJ has been predicted to be at least 1 order of magnitude less than that of state-of-the-art spin transfer torque (STT)-based memory architectures, at room temperature and with no bias fields or currents [7]. Despite the promise of high-speed, low-energy skyrmion creation and detection, there is currently no experimental evidence of skyrmions in MTJs.

One particular challenge in realizing skyrmions in MTJs is the development of unconventional detection methods.

The prevailing technique to identify skyrmion states is to directly image the magnetic configuration of the device of interest via electron or x-ray microscopy, ptychography, and magnetic force microscopy [8,9,10]. While imaging techniques give unambiguous measurements of skyrmion size and evolution, they require the magnetic layer to be exposed to a certain extent, which changes the MTJ free layer magnetic properties and limits their utility for on-chip, electrically excited skyrmion devices. Another challenge in the MTJ approach to skyrmion creation is engineering the magnetic environment necessary to induce transitions from the ferromagnetic state to a skyrmionic state in the MTJ free layer, while maintaining the requisite layer structure in the MTJ to allow for high TMR and electrical manipulation of the free layer magnetization. Normally, this may be accomplished by introducing a sufficiently strong interfacial Dzyaloshinskii-Moriya interaction (DMI) to stabilize the spin texture [11,12]. However, there is strong evidence that skyrmions can be stabilized in a confined ferromagnetic environment without the need of DMI [13,14]. Notably, a time-resolved study of current-induced switching in MTJs found that a transient magnetic bubble state is sometimes nucleated during switching and can persist for microseconds before thermal annihilation [15]. If thermal effects are suppressed, however, it is reasonable to expect that a single skyrmion can be sustained in the MTJ free layer once it is created by current-induced spin-transfer torque or voltage-controlled magnetic anisotropy [16,17].

In this Letter we show evidence that conditions for skyrmion creation inside a commercially available MTJ can be met at suitably low temperatures, and we demonstrate the electrical creation and detection of a stable nonuniform state with concurrent measurements of a MTJ's steady-state magnetoresistance and spin-polarized current-induced ferromagnetic resonance. Simulations show that the
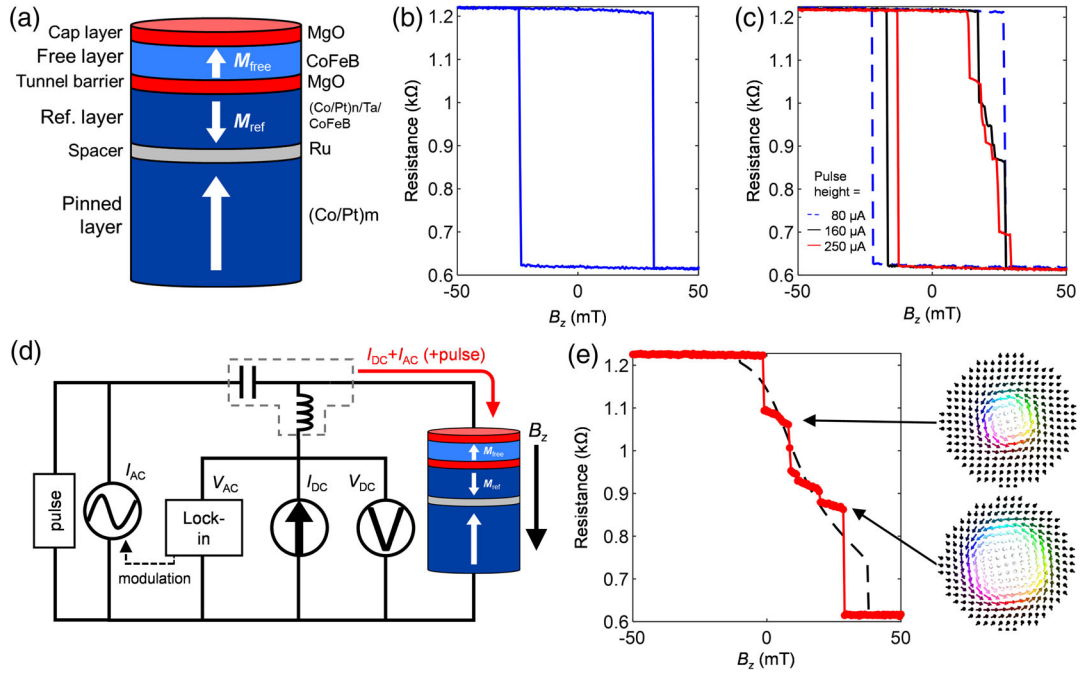
FIG. 1.   (a) MTJ layer structure. Arrows denote average magnetization of each layer at zero applied field. The positive z direction is taken to be parallel to the reference layer magnetization. (b) Out-of-plane hysteresis loop in the absence of pulsed or microwave current excitation, showing a completely perpendicular free layer magnetization. (c) Out-of-plane hysteresis loop in the presence of a repeated pulse of width 10 ns. A transition to an intermediate resistance state (IRS) appears when the pulse height exceeds 100 μA. The P $\rightarrow$ AP switching field is reduced due to the presence of spin torques. (d) Circuit diagram for magnetoresistance measurements. (e) Magnetic field dependence of the IRS with no applied excitations following initialization at 24 mT (red line) and comparison to simulations of a single skyrmion (dotted black line). Right side: snapshots of the stable skyrmion configuration at 5 (upper) and 15 mT (lower).

characteristics of this state are consistent with single skyrmion creation. We find that the electrically detected skyrmion breathing mode [18] in the resonance spectrum provides a noninvasive means for on-chip skyrmion identification.

The MTJ samples were prepared using Avalanche standard MRAM processes [19]. The magnetic layer stack was deposited using PVD and etched into nanopillars with diameters ranging from 80 to 400 nm. For this study we focus on three MTJs with 250, 350, and 400 nm diameters that all displayed qualitatively similar behavior. The MTJ layer stack and experimental setup are shown in Figs. 1(a) and 1(d). The MTJs are composed of a CoFeB-based free layer, an MgO tunneling barrier and an out-of-plane pinned synthetic antiferromagnet reference layer [24,25]. Additionally, there is a thin MgO capping layer on top of the free layer. Cryogenic testing was performed in a Janis sorption-pumped ^{3}He refrigerator.

Figure 1(b) shows a typical out-of-plane hysteresis loop of the magnetoresistance of a 250 nm MTJ in the absence of pulsed or microwave current excitation. The free layer is found to have out-of-plane magnetization at 4.2 K due to perpendicular magnetic anisotropy (PMA) induced by the MgO/CoFeB interface [26], characterized by a rectangular hysteresis loop as function of magnetic field B_z with sharp transitions between ferromagnetic states. This loop shows

the expected parallel (P) -to-antiparallel (AP) switching characteristics that are common for MTJ structures. An unexpected observation is made when a current pulse train, with a pulse width of 10 ns and a repetition rate of 100 kHz, is superimposed onto the small dc bias current. Instead of the sharp AP $\rightarrow$ P transition, an intermediate resistance state (IRS) region emerges. The width of the IRS region is a function of pulse height and it reaches 30 mT at large pulse heights. Once created, this new state persists even when the pulse is off. However, ferromagnetism is recovered when the applied field is stronger than the coercive field B_c (about 30 mT). It is important to note that the IRS is not observed for the P $\rightarrow$ AP transition.

We find that the IRS can also be deterministically created when a continuous microwave current I_{ac} is applied at selected range of frequencies f_{drive}. As shown in Fig. 2(b), the IRS is observed in the hysteresis loop for 1.3 and 1.7 GHz, for a 350 nm MTJ. When the frequency is fixed and the microwave power is decreased, the switching field gets closer to B_c and the IRS region diminishes [Fig. 2(c)]. Figure 2(a) displays a phase diagram of the IRS as a function of f_{drive} and B_z. These results are reminiscent of the well-studied microwave-assisted switching in MTJs and spin valves, where the microwave current-induced STT promotes domain nucleation in the free layer and reduces the switching energy [27]. Microwave-assisted switching is
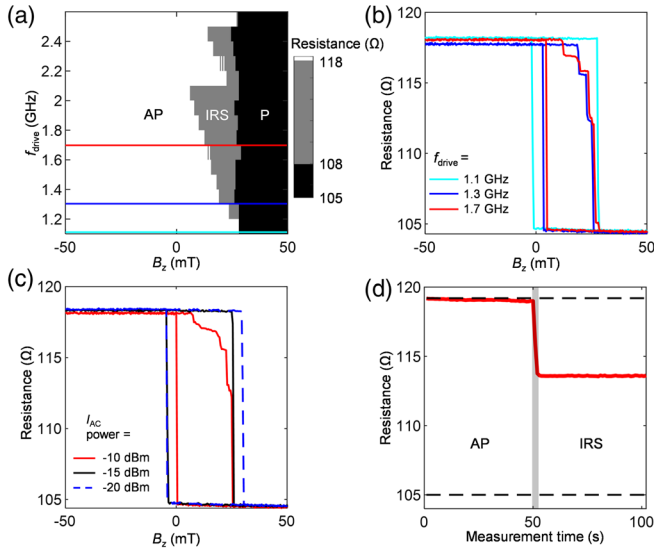
FIG. 2. (a) Inducing a transition to IRS in a 350 nm device by sweeping the magnetic field with the application of constant microwave current I_{ac}. Field scan direction is from -50 to $+50$ mT. Colored lines are cuts shown in (b). (b) A cross-sectional view of (a) including the field sweep from negative to positive values to complete the hysteresis loop. (c) Microwave power dependence on AP $\rightarrow$ IRS transition at fixed frequency $f_{drive} = 1.7$ GHz. (d) Stability of the IRS is demonstrated by applying a 1 sec I_{ac} burst (pulse applied in gray region) to transition from AP to IRS and allowing the free layer to reach static equilibrium. Static magnetic field was held at 20 mT and rf frequency $f_{drive} = 1.6$ GHz.
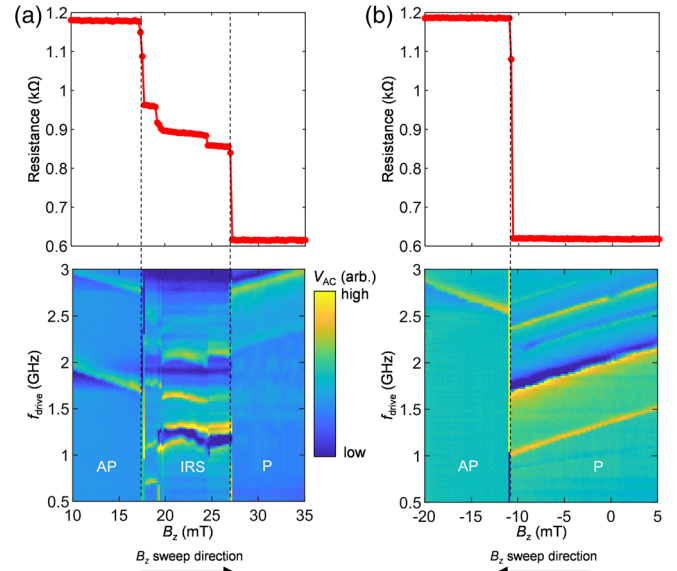

FIG. 3. Simultaneous measurement of dc resistance and magnetic resonance on the 250 nm MTJ when initialized in (a) the AP state and (b) the P state. The onset of the IRS at 17 mT in (a) is characterized by a new low-frequency mode at 1.2 GHz with a nonlinear dependence on field. In contrast, there is only a single discontinuity in the resonance spectrum representing the P $\rightarrow$ AP transition when initialized in P.

typically found to be most efficient when the microwave frequency matches a ferromagnetic resonance (FMR) mode of the free layer. As in the case with the pulse experiment, initializing the MTJ in the AP state and then briefly applying the microwave current in a one-second burst to induce the AP $\rightarrow$ IRS transition shows that the IRS is a persistent state, rather than dynamically stabilized [Fig. 2(d)].

To characterize the dynamics of the MTJ in the ferromagnetic and intermediate resistance states, we perform homodyne-detected spin-transfer driven magnetic resonance measurements [28]. An amplitude-modulated I_{ac} is mixed with a small dc current bias I_{dc} through a bias tee and applied to the MTJ. The ac component of the MTJ response V_{ac} is measured on a lock-in amplifier locked to the modulation frequency. From the results with microwave-assisted nucleation, the AP $\rightarrow$ IRS transition is expected to occur naturally as a result of the resonant driving current. A key difference between the nucleation experiment and this setup is that now the frequency is swept from the lower limit to the upper limit while the field is held fixed, so that we obtain a spectrum for each magnetic field value. The lower panel of Fig. 3(a) shows the resonance spectrum of the 250 nm device with $I_{dc} = 20$ μA, as a function of B_z. At small fields on the left side of the graph,

the MTJ is in the AP state and exhibits standard ferromagnetic resonance characterized by a linear dependence on external field and the appearance of higher-frequency spin-wave modes [29,30]. These modes have been shown to take the form of Bessel functions [31], and simulations of our devices show that they alternate between purely radial and purely azimuthal in nature [see Fig. 5(b)]. As the field is swept in the positive z direction, the microwave current induces domain nucleation and we see a discontinuity in the spectrum. While some modes appear to discretely shift, others seem to disappear entirely. At the same time, at least one new mode emerges at a lower frequency than the fundamental (uniform) ferromagnetic resonance. Increasing the field further leads to the disappearance of the low-frequency mode and the recovery of the Kittel-like FMR spectrum, now corresponding to the P state. Repeating the experiment while initialized in the P state and sweeping the field in the negative z direction shows a single discontinuity in the FMR spectrum, which is indicative of a simple transition between uniform ferromagnetic states [Fig. 3(b)].

Mixing the dc current with the driving ac current allows simultaneous measurement of the TMR during the resonance experiment (Fig. 3, upper panels). Although I_{dc} itself induces a shift in FMR frequencies, the shift is small enough that it doesn't qualitatively impact the spectra or any transitions. Recording the junction resistance during the FMR measurement confirms that the onset of the IRS exactly corresponds to the drastic change in spectrum.
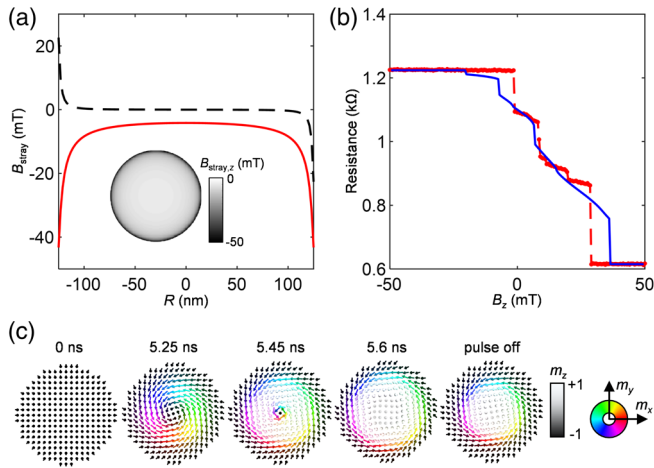
FIG. 4. (a) Simulated stray field z component (red) and x component (dotted black) seen by the free layer, along a diametric cut. Inset: spatial profile of the z component of the stray field. (b) Magnetic field dependence of the IRS (dotted red) and comparison with simulated skyrmion evolution with disorder (blue). The addition of magnetic disorder creates discontinuities in the magnetoresistance that match the observed behavior. (c) Snapshots of skyrmion formation via current pulse.

This result suggests that the IRS is a metastable, topologically nontrivial spin texture within the MTJ free layer.

To determine the nature of the nonferromagnetic IRS, we perform micromagnetic simulations of the free layer magnetization. We first compute the stray field from the magnetic layers near the free layer. Although the MTJs are designed to minimize the stray field's influence on the free layer, there may be significant torque near the nanopillar edge [32]. Simulations estimate that the free layer experiences a 50 mT out-of-plane field at the disk edge which quickly drops to less than 5 mT at the disk center. This stray field cants the spins at the edge of the disk and favors edge spins that are aligned with the stray field. The existence of this stray field is consistent with Fig. 1(b), as the MTJ displays a preference toward the antiparallel state (loop shifted in the positive B_z direction), indicating an overcompensated reference layer.

Next we simulate the behavior of the free layer when a current pulse or resonant microwave current is applied [Fig. 4(c)]. When the device is initialized in the AP state, a 10 ns current pulse exerts a torque that begins to rotate magnetic moments about a radial axis. However, the stray field makes edge spins more resistant to this rotation. Furthermore, there is no STT at the center of the disk where the spins are completely parallel to the spin polarization (in the z direction). This results in a ring of magnetic moments that experience the greatest net force from STT [second snapshot in Fig. 4(c)], and these are the first to reverse direction to form two concentric Bloch domain walls (third snapshot). The inner wall then collapses and the outer wall shrinks to form a single skyrmion (fourth and fifth snapshots). A calculation of the topological charge q of the final

state confirms that the skyrmion is very nearly quantized ($q = 0.996$, see Supplemental Material [19]). Interestingly, the predicted skyrmion is of Bloch type rather than Néel type; this is consistent with the observation that Bloch domain walls are energetically favorable over Néel walls in ferromagnetic thin films with PMA and vanishing DMI [33]. We expect the DMI to be negligible in our devices, since the free layer is sandwiched between MgO layers. The symmetry of the adjacent materials mostly cancels out any small DMI that could arise from the MgO/CoFeB interface [34]. Simulating the free layer in the presence of a persistent microwave current tuned to match ferromagnetic resonance shows a qualitatively similar skyrmion transition.

The magnetic field dependence of the IRS in experiments is also consistent with the skyrmion picture. As the field is swept through the IRS, the initially small skyrmion (estimated to be 75 nm in diameter at its smallest, near zero field) grows larger and the average M_z is reduced. This leads to a decrease in resistance, until the skyrmion expands to the boundary of the disk and turns into the P state. Simulations of a skyrmion evolving in this way are consistent with the observed TMR curve [Fig. 1(d)], with one discrepancy: measurements show discrete steps in the magnetoresistance curve. When magnetic disorder is incorporated into the simulation, the magnetoresistance curve acquires steps similar to the observed behavior [Fig. 4(b), see Supplemental Material [19] for details] [35].

The dynamics of the skyrmion can be experimentally inferred from the IRS resonance spectrum. At IRS onset, the ferromagnetic resonance modes vanish and a large negative peak appears near 1 GHz. Simulations based on material parameters extracted from FMR identify this mode as the breathing mode, or expansion and contraction of the skyrmion [Figs. 5(a), 5(b)]. The breathing mode is a ubiquitous characteristic of skyrmions and has a complex dependence on external fields [18]. If the skyrmion core is aligned with the reference layer, as is the case in these devices, then a positive (negative) current causes skyrmion expansion (contraction) and consequently a negative peak in the spectrum. In further contrast with ferromagnetic resonance lines, which show substantial asymmetry due to the current-induced fieldlike torque, the skyrmion breathing mode is mostly symmetric [Figs. 5(c), 5(d)]. Simulations of the resonant frequency profile agree well with the observed profiles [Figs. 5(c), 5(d) insets].

The MTJ can be a powerful tool to create and sense skyrmions in magnetic films. Our results show that a single skyrmion with a diameter smaller than 100 nm can cause a change in junction resistance of almost 10%, which is more than sufficient for electrical detection. We can also conclude that the energy cost for current-induced skyrmion creation is less than the energy of full ferromagnetic switching since the transition to a skyrmion state occurs at lower applied field in pulse experiments.
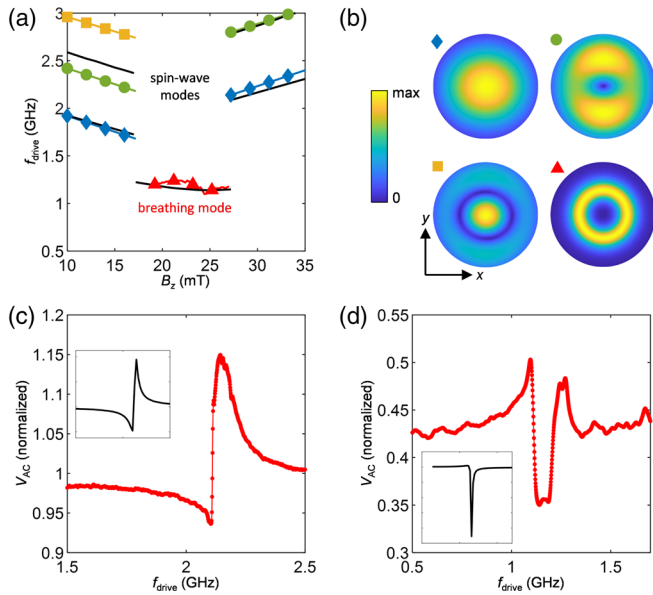
FIG. 5. (a) The magnetic resonance landscape of the 250 nm device from Fig. 3 (colored symbols) and comparison to simulations (solid black lines). (b) Corresponding spatial profiles of ferromagnetic spin-wave mode amplitudes showing alternating radial (blue diamonds, yellow squares) and azimuthal (green circles) modes. Also shown is the skyrmion breathing mode (red triangles). Profiles for the FM (skyrmion) states were obtained from the Fourier transform of m_x (m_z) dynamics for each cell in the simulation. (c) Frequency profile of the first FMR mode taken at 5 mT in the AP state. (d) Frequency profile of the skyrmion breathing mode taken at 20 mT. Insets are simulated profiles.

Unlike the prevailing imaging techniques, pure electrical detection only provides indirect evidence of a skyrmion state. It is therefore critical that the magnetoresistance and the magnetic resonance spectrum are mutually consistent to discriminate skyrmions from other spin textures. As demonstrated in the Supplemental Material Fig. S3 [19], the magnetoresistance curve of a single skyrmion is qualitatively similar to the magnetoresistance that would arise from the formation of a generic magnetic bubble. However, the skyrmion breathing mode frequency is expected to be an order of magnitude higher than the fundamental mode of a bubble, which emphasizes the need for resonance measurements. In addition to theoretical considerations, our experimental observations are qualitatively distinct from other published work on domains and defects in magnetic nanostructures [36,37].

To conclude, we have experimentally demonstrated the deterministic electrical switching of a MTJ free layer from a ferromagnetic state to a nontrivial spin texture. Micromagnetic simulations, using our device parameters, strongly suggest that this texture is a single skyrmion created in the free layer, facilitated by the reference layer stray field that favors spins at the pillar edge to be canted away from the bulk magnetization. This work could lead to purely electrical creation, detection, and characterization of skyrmions in MTJs for memory and computational applications.

*Corresponding author.
jiangh@physics.ucla.edu

[1] A. Fert, N. Reyren, and V. Cros, Magnetic skyrmions: Advances in physics and potential applications, Nat. Rev. Mater. **2,** 17031 (2017).

[2] X. Zhang, M. Ezawa, and Y. Zhou, Magnetic skyrmion logic gates: Conversion, duplication and merging of skyrmions, Sci. Rep. **5,** 9400 (2015).

[3] Y. Huang, W. Kang, X. Zhang, Y. Zhou, and W. Zhao, Magnetic skyrmion-based synaptic devices, Nanotechnology **28,** 08LT02 (2017).

[4] G. Yang, P. Stano, J. Klinovaja, and D. Loss, Majorana bound states in magnetic skyrmions, Phys. Rev. B **93,** 224505 (2016).

[5] W. Koshibae, Y. Naneko, J. Iwasaki, M. Kawasaki, Y. Tokura, and N. Nagaosa, Memory functions of magnetic skyrmions, Jpn. J. Appl. Phys. **54,** 053001 (2015).

[6] W. Kang, Y. Huang, C. Zheng, W. Lv, N. Lei, Y. Zhang, X. Zhang, Y. Zhou, and W. Zhou, Voltage controlled magnetic skyrmion motion for racetrack memory, Sci. Rep. **6,** 23164 (2016).

[7] D. Bhattacharya, M. M. Al-Rashid, and J. Atulasimha, Voltage controlled core reversal of fixed magnetic skyrmions without a magnetic field, Sci. Rep. **6,** 31272 (2016).

[8] S. Pollard, J. Garlow, J. Yu, Z. Wang, Y. Zhu, and H. Yang, Observation of stable Neel skyrmions in cobalt/palladium multilayers with Lorentz transmission electron microscopy, Nat. Commun. **8,** 14761 (2017).

[9] Y. Onose, Y. Okamura, S. Seki, S. Ishiwata, and Y. Tokura, Observation of magnetic excitations of skyrmion crystal in a helimagnetic insulator Cu_2OSeO_3, Phys. Rev. Lett. **109,** 037603 (2012).

[10] M. Schott, A. Bernand-Mantel, L. Ranno, S. Pizzini, J. Vogel, H. Bea, C. Baraduc, S. Auffret, G. Gaudin, and D. Givord, The skyrmion switch: turning magnetic skyrmion bubbles on and off with an electric field, Nano Lett. **17,** 3006 (2017).

[11] A. Bogdanov and U. Rößler, Chiral symmetry breaking in magnetic thin films and multilayers, Phys. Rev. Lett. **87,** 037203 (2001).

[12] O. Boulle, J. Vogel, H. Yang, S. Pizzini, D. d. S. Chavez, A. Locatelli, T. O. Mentes, A. Sala, L. Buda-Prejbeanu, O. Klein, M. Belmeguenai, Y. Roussigne, A. Stashkevich, S. M. Cherif, L. Aballe, M. Foerster, M. Chshiev, S. Auffret, I. M. Miron, and G. Gaudin, Room-temperature chiral magnetic skyrmions in ultrathin magnetic nanostructures, Nat. Nanotechnol. **11,** 449 (2016).

[13] Y. Dai, H. Wang, P. Tao, T. Yang, W. Ren, and Z. Zhang, Skyrmion ground state and gyration of skyrmions in magnetic nanodisks without the Dzyaloshinsky-Moriya interaction, Phys. Rev. B **88,** 054403 (2013).

[14] K. Guslienko, Skyrmion state stability in magnetic nanodots with perpendicular anisotropy, IEEE Magn. Lett. **6,** 1 (2015).

[15] T. Devolder, A. L. Goff, and V. Nikitin, Size dependence of nanosecond-scale spin-torque switching in perpendicularly magnetized magnetic tunnel junctions, Phys. Rev. B. **93,** 224432 (2016).

[16] J. Sampaio, V. Cros, S. Rohart, A. Thiaville, and A. Fert, Nucleation, stability, and current-induced motion of isolated magnetic skyrmions in nanostructures, Nat. Nanotechnol. **8,** 839 (2013).

[17] Y. Nakatani, M. Hayashi, S. Kanai, S. Fukami, and H. Ohno, Electric field control of skyrmions in magnetic nanodisks, Appl. Phys. Lett. **108,** 152403 (2016).

[18] J.-V. Kim, F. Garcia-Sanchez, J. Sampaio, C. Moreau-Luchaire, V. Cros, and A. Fert, Breathing modes of confined skyrmions in ultrathin magnetic dots, Phys. Rev. B **90,** 064410 (2014).

[19] See Supplemental Material at http://link.aps.org/supplemental/10.1103/PhysRevLett.122.257201 for MTJ stack details, data on additional devices, and simulation methods, etc., which includes Refs. [20–23].

[20] A. Vansteenkiste, J. Laliaert, M. Dvornik, M. Helsen, F. Garcia-Sanchez, and B. V. Waeyenberge, The design and verification of MuMax3, AIP Adv. **4,** 107133 (2014).

[21] S. Heinz, K. v. Bergmann, M. Menzel, J. Brede, A. Kubetzka, R. Weisendanger, G. Bihlmayer, and S. Blugel, Spontaneous atomic-scale magnetic skyrmion lattice in two dimensions, Nat. Phys. **7,** 713 (2011).

[22] S. M. Mohseni, S. R. Sani, J. Persson, T. N. A. Nguyen, S. Chung, Y. Pogoryelov, P. K. Muduli, E. Iacocca, A. Eklund, R. K. Dumas, S. Bonetti, A. Deac, M. A. Hoefer, and J. Akerman, Spin torque-generated magnetic droplet solitons, Science **339,** 1295 (2013).

[23] X. Zhang, W. Cai, X. Zhang, Z. Wang, Z. Li, Y. Zhang, K. Cao, N. Lei, W. Kang, Y. Zhang, H. Yu, Y. Zhou, and W. Zhou, Skyrmions in magnetic tunnel junctions, ACS Appl. Mater. Interfaces **10,** 16887 (2018).

[24] S. Parkin, N. More, and K. Roche, Oscillations in exchange coupling and magnetoresistance in metallic superlattice structures: Co/Ru, Co/Cr, and Fe/Cr, Phys. Rev. Lett. **64,** 2304 (1990).

[25] H. Gan, R. Malmhall, Z. Wang, B. K. Yen, J. Zhang, X. Wang, Y. Zhou, X. Hao, D. Jung, K. Satoh, and Y. Huai, Perpendicular magnetic tunnel junction with thin CoFeB/Ta/Co/Pd/Co reference layer, Appl. Phys. Lett. **105,** 192403 (2014).

[26] S. Ikeda, K. Miura, H. Yamamoto, K. Mizunuma, H. Gan, M. Endo, S. Kanai, J. Hayakawa, F. Matsukura, and H. Ohno, A perpendicular-anisotropy CoFeB-MgO magnetic tunnel junction, Nat. Mater. **9,** 721 (2010).

[27] H. Suto, T. Nagasawa, K. Kudo, K. Mizushima, and R. Sato, Microwave-assisted switching of a single perpendicular magnetic tunnel junction nanodot, Appl. Phys. Express **8,** 023001 (2015).

[28] J. Sankey, P. Braganca, A. Garcia, I. Krivorotov, R. Buhrman, and D. Ralph, Spin-transfer-driven ferromagnetic resonance of individual nanomagnets, Phys. Rev. Lett. **96,** 227601 (2006).

[29] A. Helmer, S. Cornelissen, T. Devolder, J.-V. Kim, W. v. Roy, L. Lagae, and C. Chappert, Quantized spin-wave modes in magnetic tunnel junction nanopillars, Phys. Rev. B **81,** 094416 (2010).

[30] Z. Zeng, K. Cheung, H. W. Jiang, I. Krivorotov, J. Katine, V. Tiberkevich, and A. Slavin, Evolution of spin-wave modes in magnetic tunnel junction nanopillars, Phys. Rev. B **82,** 100410 (2010).

[31] V. Naletov, G. d. Loubens, G. Albuquerque, S. Borlenghi, V. Cros, G. Faini, J. Grollier, H. Hurdequint, N. Locatelli, B. Pigeau, A. Slavin, V. Tiberkevich, C. Ulysse, T. Valet, and O. Klein, Identification and selection rules of the spin-wave eigenmodes in a normally magnetized nanopillar, Phys. Rev. B **84,** 224423 (2011).

[32] D. Gopman, D. Bedau, S. Mangin, C. Lambert, E. Fullerton, J. Katine, and A. Kent, Asymmetric switching behavior in perpendicularly magnetized spin-valve nanopillars due to the polarizer dipole field, Appl. Phys. Lett. **100,** 062404 (2012).

[33] M. Benitez, A. Hrabec, A. Mihai, T. Moore, G. Burnell, D. McGrouther, C. Marrows, and S. McVitie, Magnetic microscopy and topological stability of homochiral Neel domain walls in a Pt/Co/AlOx trilayer, Nat. Commun. **6,** 8957 (2015).

[34] C. Moreau-Luchaire, C. Moutafis, N. Reyren, J. Sampaio, C. A. F. Vaz, N. V. Horne, K. Bouzehouane, K. Garcia, C. Deranlot, P. Warnicke, P. Wohlhuter, J.-M. George, M. Weigand, J. Raabe, V. Cros, and A. Fert, Additive chiral interfacial interaction in multilayers for stabilization of small individual skyrmions at room temperature, Nat. Nanotechnol. **11,** 444 (2016).

[35] R. Juge, S.-G. Je, D. d. S. Chavez, S. Pizzini, L. Buda-Prejbeanu, L. Aballe, M. Foerster, A. Locatelli, T. Mentes, A. Sala, F. Macherozzi, S. Dhesi, S. Auffret, E. Gautier, G. Gaudin, J. Vogel, and O. Boulle, Magnetic skyrmions in confined geometries: effect of the magnetic field and the disorder, J. Magn. Magn. Mater. **455,** 3 (2018).

[36] S. Ingvarsson, G. Xiao, S. S. P. Parkin, W. J. Gallagher, G. Grinstein, and R. H. Koch, Low-frequency magnetic noise in micron-scale magnetic tunnel junctions, Phys. Rev. Lett. **85,** 3289 (2000).

[37] D. Ravelosona, S. Mangin, Y. Lemaho, J. A. Katine, B. D. Terris, and E. E. Fullerton, Domain wall creation in nano-structures driven by a spin-polarized current, Phys. Rev. Lett. **96,** 186604 (2006).